JOURNAL OF AIRCRAFT
Vol. 47, No. 3, May–June 2010

Engineering Notes

Investigation into the Aerodynamic Performance of the Tiltrotor Unmanned Aerial Vehicle Proprotor

Seong Wook Choi* and Jai Moo Kim†
Korea Aerospace Research Institute, Daejeon 305-333, Republic of Korea

DOI: 10.2514/1.47533

I. Introduction

THE Smart UAV is a tilt-rotor type of convertiplane, which can take off and land like a helicopter and convert to a propeller-driven fixed-wing aircraft through a tilting procedure. Therefore, unlike the propeller of a conventional fixed-wing aircraft or the rotor of a helicopter, the proprotor of a tilt-rotor aircraft experiences significant changes in aerodynamic loading during its overall flight modes. The differences in aerodynamic performance due to tilt angle and forward speed cause severe changes in thrust and moments. They may also induce significant vibration due to asymmetric flow on the rotor disk. To evaluate the aerodynamic performance of the rotor under such varying flight conditions, numerical simulations and experimental tests were conducted in this study.

The geometric specifications and operating conditions of the proprotor of a full-scale Smart UAV are summarized in Tables 1 and 2, respectively [1], and the computational grid and sign convention of the proprotor are shown in Fig. 1.

This paper includes three parts. Section II describes the unsteady numerical simulation of airflow around the proprotor using Navier–Stokes equations with a dynamic overset grid technique. Section III introduces the structure of the proprotor test rig and the results of the ground test. And in Sec. IV, the results of the wind-tunnel test, conducted in a low-speed wind tunnel at the Korea Aerospace Research Institute, are discussed using a comparison with the numerical data mentioned in Sec. II. For all numerical and experimental tests in this study, the hub of the proprotor was modeled and fabricated as a rigid hub. In the interest of simplicity and cost effectiveness, the hub has no cyclic pitch control in either test.

II. Numerical Flow Analysis

A numerical simulation was conducted for investigating the aerodynamic performance of the isolated proprotor, which was composed of three blades and a nacelle. The flow calculation around the proprotor was performed using CFD-FASTRAN [2]. Figure 1 shows the dynamic overset grid system, which was composed of three rotating blade grids and a stationary nacelle grid. The flow condition was set based on the flight scenario of the Smart UAV. The calculation uses the Reynolds-averaged compressible Navier–Stokes equations with the Spalart–Allmaras turbulence model. Roe's flux-difference splitting for spatial difference and the fully implicit time integration method were applied for the unsteady calculation.

The unsteady calculations were conducted for three flight modes as categorized in Table 3. Among those three flight modes, the calculation results of the hover and airplane modes were compared with the results from the in-house prediction code based on blade element momentum theory (BEMT) [3]. The conditions of tilt were simulated by varying angles of freestream (θ in Fig. 1) instead of tilting grids.

The calculations for the hover and airplane modes serve two purposes: acquiring the aerodynamic performance and verifying the numerical analysis using a comparison with the result of the BEMT. For the hover mode, both the inviscid and viscous flow calculations were performed and the difference due to viscous effect was investigated.

Figure 2 shows the curves of thrust coefficient C_T and torque coefficients C_Q for the variation of collective pitch at the 75% blade radius, which were compared with the predicted result of the BEMT for hover mode. The thrust coefficient curve of CFD-FASTRAN

Table 1 Geometry of proprotor

Geometry						
No. of blades	3		Solidity (σ_T)		0.118	
Radius, ft	4.7		Activity factor		93.8	
Diameter, ft	9.4		Taper ratio		0.64	
Disk loading, lb/ft^2	15.0		Equiv. Chord (Ft)		0.58	
Disk area, ft^2	69.4		Root(0.1 R) Chord(ft)		0.785	
Blade area, ft^2	2.7		Tip(1.0 R) Chord(ft)		0.503	
Thickness ratio	r/R	0.10	0.25	0.50	0.75	1.00
	t/c	0.30	0.25	0.18	0.12	0.08
Blade twist	38 deg (32 deg @ 0.1R, −6 deg @ 0.1R)					

Table 2 Operating condition of proprotor

Operating condition	Hover (SLS, ISA, $V = 0$ kt)	Cruise (10 kft, ISA, $V = 270$ kt)	Reduction ratio
Rpm	1605	1284	0.8
V_{tip}, fps	790	632	——
M_{tip}	0.71	0.59	——

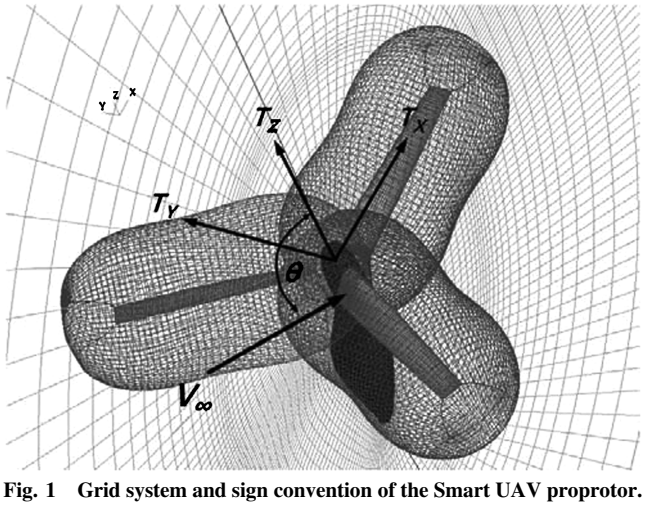

Fig. 1 Grid system and sign convention of the Smart UAV proprotor.

Received 17 October 2009; revision received 12 January 2010; accepted for publication 1 February 2010.

*Head, Air Vehicle Systems, Smart UAV Development Center. Member AIAA.
†Director, Smart UAV Development Center.

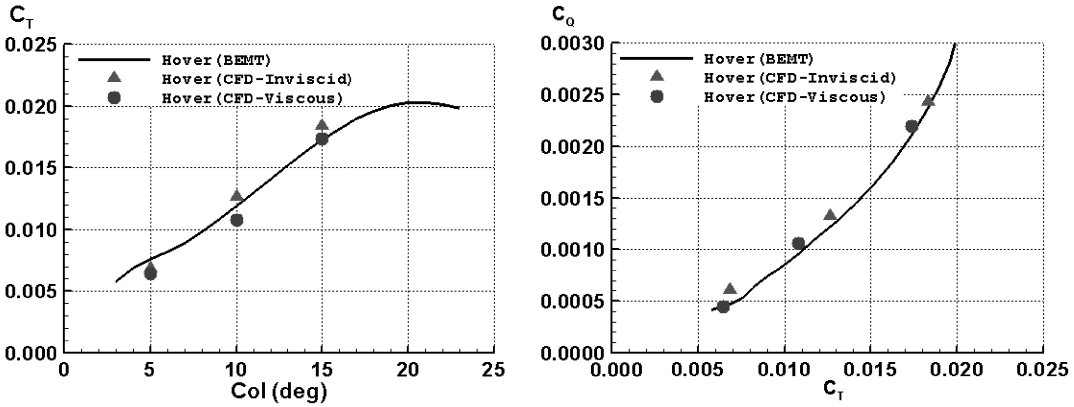

Fig. 2 Hover mode performance: a) Col-C_T, and b) $C_T - C_Q$.

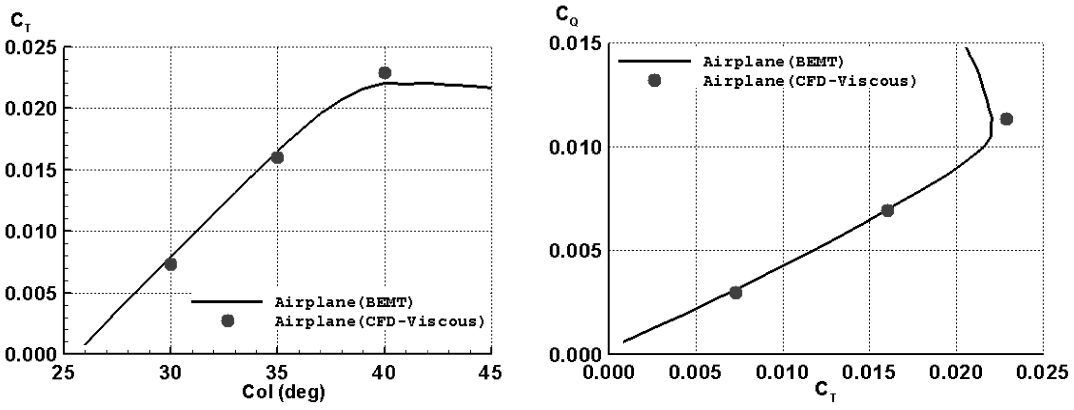

Fig. 3 Airplane mode performance: a) Col-C_T, and b) $C_T - C_Q$.

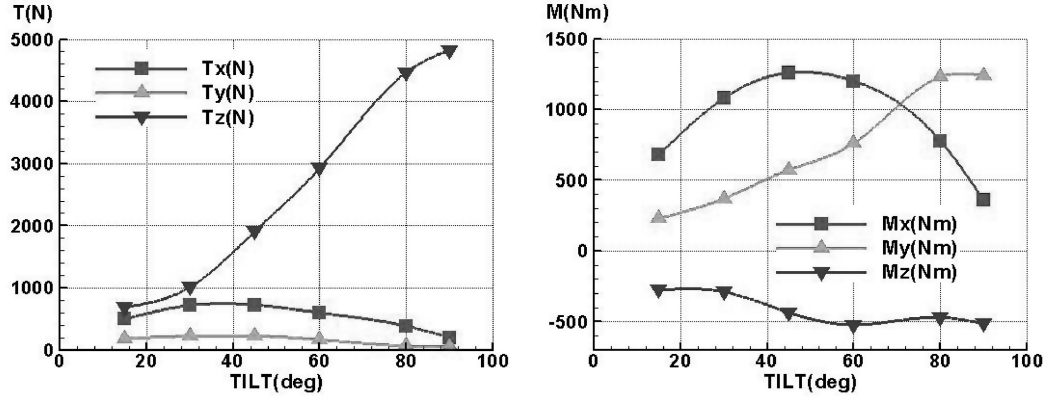

Fig. 4 Conversion mode performance (CFD-FASTRAN-Viscous): a) TILT–thrust, and b) TILT–moment.

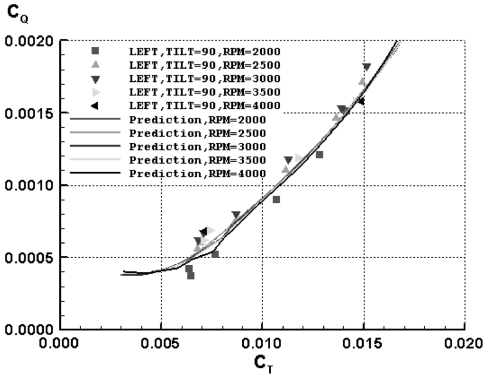

Fig. 5 $C_T - C_Q$ curves from the ground test and BEMT.

Fig. 6 Proprotor test rig installed in the wind tunnel.

Table 3 Flight and wind-tunnel test condition

	Flight Condition				Test Condition			
Mode	Tilt, deg	Col, deg	Speed, km/h	Rpm	Advance ratio	Col, deg	Speed, m/s	Rpm
Hover	90	10	0	1605	0.00	10	0	4012
	90	7.7	60	1605	0.07	8	15	3610
	80	6.2	133	1605	0.15	6	25	2705
	60	9.4	188	1605	0.22	10	30	2308
Conversion	45	12.6	202	1605	0.23	12	40	2860
	30	15.7	216	1605	0.25	16	40	2676
	15	18.4	231	1605	0.27	18	40	2500
	0	20.5	250	1605	0.29	20	40	2310
Airplane	0	28.0	250	1284	0.36	28	40	1850

shows good agreement with the predicted result. However, the thrust coefficient of the inviscid calculation appears higher than in the case of the viscous calculation. The thrust coefficient and torque coefficient curves also show overall agreement with prediction data. For the airplane mode, only the viscous calculation was conducted, as shown in Fig. 3. The collective pitch versus thrust coefficient curve shows favorable agreement with the prediction data, though some discrepancies were found at higher pitch angles. Although the prediction by BEMT shows stall characteristics, the computation data tend to remain linear up to the higher pitch angles. The thrust–torque curve also shows good agreement except at the higher pitch angles.

Figure 4 shows thrust and moment components calculated from the CFD-FASTRAN in the conversion mode. The normal thrust component Tz increased with the increase of tilt angle and horizontal force. In addition, the figure shows that the axial thrust Tx is higher than the side force Ty due to the effect of freestream direction. The figure implies that the axial thrust Tx equals the side force Ty at a tilt angle of 0 deg with the difference growing with tilt angle. For moments of rotor hub, the pitch up moment My increases with tilt angle and hits its maximum value at a tilt angle of 90 deg, and the roll moment Mx reaches its maximum around a tilt angle of 45 deg.

III. Proprotor Test Rig and Ground Test

The proprotor of the power test rig was built to 40% scale of the Smart UAV. The test was based on the Mach scale test, which sets the maximum rotational speed of the scaled proprotor to 4012 rpm in hover mode. The ground test for the proprotor was conducted to evaluate the safety of the system, to perform dynamic balancing of the hub, to investigate the vibration level, and to obtain aerodynamic performance in hover.

The test rig of the 40% scale proprotor was composed of proprotors, electric motors, supports and tilting structures, power and cooling systems, and a control system. An induction-type, water-cooling, geared motor capable of 50 hp and 4012 rpm was used to drive the proprotor. A force component (Tz) and two moment components (Mx, My) of the proprotor hub were measured by four load cells installed in the front section of the motor assembly.

Four aerodynamic forces and moments of the proprotor were obtained in this ground test: a thrust and two moments measured from the rotor balance system, and a rotor power converted from the electric power of the motor. Of those components, mostly due to asymmetry in flow and tilt conditions, the two hub moments Mx and My were so small as to be negligible in a ground test involving no forward speed at all. The test data were compared with the prediction data from the BEMT. Figure 5 displays the thrust coefficient versus torque coefficient curve and shows good agreement with prediction data.

IV. Wind-Tunnel Test

After the ground test of the proprotor mentioned in Sec. III, the test rig was installed in the wind tunnel and the test was conducted for the forward flight condition. Next, the wind-tunnel test result was compared with the numerical and predicted data and the accuracy was assessed for both.

The proprotor power test rig, which would eventually be used in the powered wind-tunnel test for the full configuration of the Smart UAV, was installed in the wind tunnel as shown in Fig. 6. The test rig was installed on the turntable of the wind-tunnel test section to enable a yawing test. In addition, a number of tufts were attached to the wind-tunnel floor to investigate flow pattern at the high tilting angle in which flow breakdown might occur.

The wind-tunnel test condition, as shown in Table 3, was set up based on the flight conditions of the Smart UAV and the rotational speed of the scaled rotor, which was in turn obtained by using similar advance ratios as the full-scale air vehicle. The hover mode in which the advance ratio is zero could not be conducted in this test because of flow reingestion into the rotor, due to the closed wall of the wind-tunnel test section.

Figure 7 shows the variation of thrust and power with the increase of wind speed for the airplane mode under the conditions of 0 deg tilt and 28 deg collective pitch. The data were then compared with the prediction data. As the forward speed increases, the thrust decreases

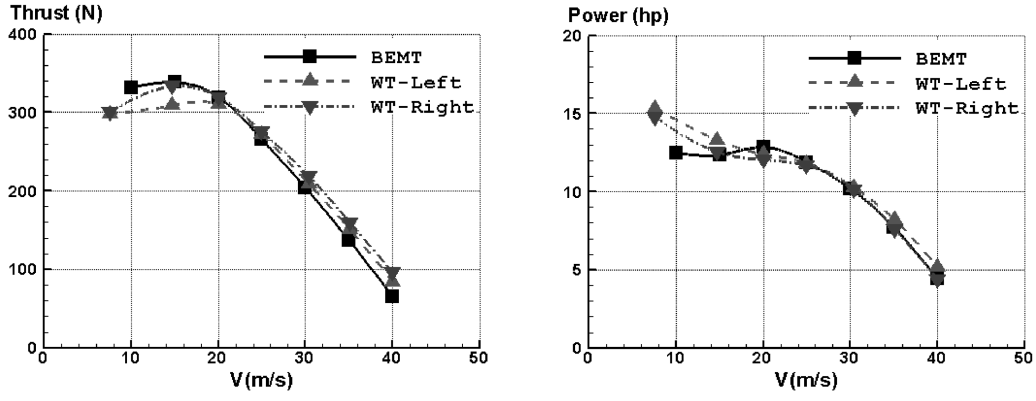

Fig. 7 Thrust and power variations for wind speed (tilt = 0, col = 28, rpm = 1850).

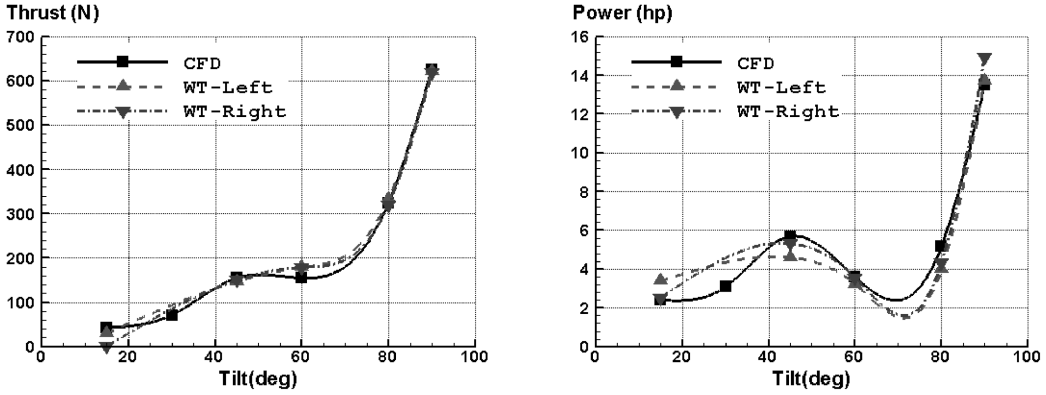

Fig. 8 Thrust and power variation for tilt.

and finally reaches windmill state at a wind speed of 45 m/s. On the other hand, thrust decrease due to blade stall was observed at wind speeds below 20 m/s.

Figure 8 shows rotor performance for the conversion mode as listed in Table 3, and the result was compared with data from the numerical calculation (CFD-FASTRAN). The thrust increases as tilt angle increases, and the results show good agreement with CFD-FASTRAN data. The power of the rotor has a higher value near a tilt angle of 45 deg and hits its maximum at 90 deg of tilt.

V. Conclusions

In summary, numerical and experimental investigations have been conducted on an isolated proprotor in the full configuration of the tilt-rotor Smart UAV, fabricated for the powered wind-tunnel test. The aerodynamic performance obtained from the ground and wind-tunnel tests was compared with the calculated data from the CFD-FASTRAN and BEMT methods and shows overall good agreement.

Using the numerical analysis of the proprotor, this paper has shown the applicability of engineering data and the possibility of unsteady flow calculations for the proprotor in hover, conversion, and airplane modes. Moreover, the numerical study indicates the potential for calculations of a powered full configuration with the proprotor. Even though all the tests were conducted for the proprotor with a rigid hub, the aerodynamic data of the scaled proprotor obtained in this study may not only be used for the investigation of the aerodynamic performance of the isolated proprotor, but may also be compared with the powered wind-tunnel data for a full configuration vehicle to extract the aerodynamic effect due to a proprotor.

Acknowledgment

This research was performed for the Smart UAV Development Program, one of the 21st Century Frontier R&D Programs funded by the Ministry of Knowledge and Economy of Korea.

References

[1] Choi, S. W., Kim, Y. S., Park, Y. M., and Kim, J. M., "Aerodynamic Design of the SUAV Proprotor," *Journal of the Korean Society for Aeronautical Space Science*, Vol. 33, No. 9, 2005. pp 16–26.

[2] CFD-FASTRAN User Manual, Ver. 2003, CFD Research Corp., Huntsville, AL, 2003.

[3] Choi, S. W., Kim, Y. S., and Kim, J. M., "Performance Analysis of the Hovering/Cruise Mode of Proprotor," *Proceedings of the KSAS Spring Conference*, Korean Society for Aeronautical Space Sciences, Kyungju, Korea, Nov. 2003, pp. 700–705.